Article:
Bergenti, Ilaria, Riminucci, Alberto, Graziosi, Patrizio et al. (2021) Spinterface Formation at α-Sexithiophene/Ferromagnetic Conducting Oxide. Journal of Physical Chemistry C. pp. 6073-6081. ISSN: 1932-7455

https://doi.org/10.1021/acs.jpcc.0c09713

Spinterface formation at α-sexithiophene/ ferromagnetic conducting oxide

I. Bergenti[1], A. Riminucci[1], P. Graziosi[1], C. Albonetti[1], M. Benini[1], S. Toffanin[1], S. Lopez[1], R. K. Rakshit [2], Manju Singh[2], P. D. Bentley[3], I. A. Melchakova[4], P. V. Avramov[4], V. A. Dediu[1], and A. Pratt[3]

[1]Institute of Nanostructured Materials ISMN-CNR, via Gobetti 101, 40129 Bologna, Italy

[2]CSIR - National Physical Laboratory, Dr. K. S. Krishnan Marg, New Delhi, 110012, India

[3] Department of Physics, University of York, Heslington, York, YO10 5DD, UK

[4] Department of Chemistry, Kyungpook National University, 80 Daehak-ro, Buk-gu, Daegu, 41566, South Korea

ABSTRACT:

The inorganic/molecular spinterface is an ideal platform for generating extraordinary spin effects. Understanding and controlling these spin-related effects is mandatory for the exploitation of such interfaces in devices. For this purpose, we have investigated the adsorption of α-sexithiophene (α-6T) on $La_{0.7}Sr_{0.3}MnO_3$ (LSMO), as one of the prototypical material combinations used in organic spintronic devices. Atomic force microscopy, confocal photoluminescence, X-ray photoelectron spectroscopy, and metastable de-excitation spectroscopy unraveled the structure and electronic configuration of 6T for various surface coverages. This data set allowed the determination of characteristic features of occupied states, the band diagram and the work function. Finally, density functional theory enabled us to establish that the spin polarization in 6T molecular orbitals critically depends on the termination layer of LSMO. We believe that this research provides important hints for a comprehensive understanding of spinterface effects in general and provides key suggestions for further engineering of LSMO/6T-based devices.

INTRODUCTION:

Hybridization at the interface between molecular entities and ferromagnetic metals leads to drastic changes of the properties of both layers [1,2]. Notably, an increase of spin polarization of states around the Fermi level [2], modulation of the magnetic anisotropy [3] and spin re-orientation transitions were observed in ferromagnetic layers as well as the appearance of spin polarized states in the molecular material [5]. Such new hybrid interfaces with unexpected spin functionality, named after the seminal paper by Sanvito as “spinterfaces” [6], act as a key element at the molecular level for engineering the properties and the performance of spin-devices. Among the plethora of spinterfaces, those including half-metallic ferromagnetic oxides such as $La_{0.7}Sr_{0.3}MnO_3$(LSMO) are of special interest. LSMO has been coupled to a variety of organic molecules and successfully used in spintronic devices [7,8], even showing the inversion of the sign of the polarization upon the deposition of an organic molecule [9]. Nonetheless, the variability of the composition of the termination layer of LSMO [10–12] hindered a reliable investigation of its interface with organic molecules. In this paper we focus on the coupling between a π-conjugated oligothiophene, 6T (sexithiophene), and LSMO; one of the first hybrid interfaces used in spin injection devices [13]. 6T is a rod-like model organic molecule [14] which contains six thiophene rings linked together; it can be easily sublimated in ultrahigh vacuum (UHV), a pre-requisite for the control and reproducibility of interfacial states, and it is also known to form ordered thin layers on solid surfaces. Here, the growth process of 6T on

LSMO has been studied by photoemission spectroscopy and metastable helium de-excitation spectroscopy to follow the evolution of spectral signatures as a function of coverage. The complementary investigation of morphology by atomic force microscopy (AFM) and molecule-LSMO coupling by confocal microscopy allows a full description of the 6T/LSMO interaction. First principles calculations based on density functional theory (DFT) help to bridge the gap between the experimental reports on molecular orientation, binding energies, and heights, in addition to the electronic structure of the interface. Our results demonstrate that the interface is characterized by a weak electronic coupling but that, nonetheless, spin polarization extends over the 6T molecule allowing spin polarized injection.

EXPERIMENTAL

Epitaxial $La_{0.7}Sr_{0.3}MnO_3$ (LSMO) films were grown on a single crystal $SrTiO_3$ (100) substrate by channel spark ablation (CSA) from a stoichiometric polycrystalline target [15]. Substrate temperature was kept close to 880 °C in an oxygen pressure of $P=4\times10^{-2}$ mbar. LSMO films were then transferred to a UHV system (base pressure of $<2\times10^{-10}$ mbar) to perform surface analysis and the deposition of organic material. To recover surface quality and remove the contamination due to air exposure, LSMO films were subjected to a mild anneal at 250 °C following the procedure described in Refs. [8] and [10] with optimal surface quality confirmed by ultraviolet photoelectron spectroscopy (UPS) and X-ray photoelectron spectroscopy (XPS). During the evaporation of 6T (Sigma-Aldrich), the LSMO temperature (T_{sub}) was held at 120 °C and the deposition rate was 0.02 Å/s. The total quantity of organic material deposited on the LSMO was evaluated by using a room temperature quartz microbalance. UPS experiments were conducted using a He discharge source at photon energies of 21.2 eV with a monochromated Al Kα source at 1486.6 eV (XM1000, Scienta Omicron GmbH) used to perform XPS. Metastable de-excitation spectroscopy (MDS) was performed using a helium 2^3S beam generated using a cold-cathode DC discharge source [16]. The cross-section for de-excitation of He 2^3S atoms at a sample surface is sufficiently large to ensure there is zero penetration below the topmost layer providing extreme surface sensitivity when compared to UPS and XPS which provide information averaged over at least several atomic layers. All three electron spectroscopies were performed in the same UHV chamber with emitted electrons detected using a hemispherical energy analyzer (Scienta Omicron EA 125).

The topography of 6T films was investigated by using an AFM Smena microscope (NT-MDT, Moscow, Russia) in Intermittent Contact Mode (ICM) under ambient conditions. The silicon cantilevers employed in ICM measurements (NSG11, NT-MDT, Moscow, Russia) had nominal resonant frequency, ω_0, of ~150 and ~240kHz and spring constant, k, of ~5 and ~12 N/m, respectively. The 6T molecular packing was explored by confocal photoluminescence (PL) microscopy with images obtained using a Nikon Eclipse TE-2000-E fluorescence confocal microscope and excitation light provided by a 488 nm Ar^+ laser. A 405/488 nm dual dichroic mirror reflected the excitation beam towards a 60× air objective (N.A.=1.4).

All electronic structure calculations were performed using the Vienna Ab-initio Simulation Package (VASP) [17–20] within the DFT framework. A plane wave basis set with the projector augmented wave (PAW) method [21,22] and the GGA-PBE functional [23,24] taking into account Hubbard corrections (GGA + U) [25,26] and the Grimme correction [27] for van der Waals interactions were used. Monkhorst-Pack Brillouin zone k-point sampling was implemented, and the k-point mesh contained 2×2×1 k-points for the corresponding supercells. A vacuum interval of 20 Å was set normal to the plane to avoid artificial interactions between adjacent images. The cutoff energy was equal to 400 eV. A maximum force acting on atoms less than 0.001 eV/Å was used as a stopping criterion for structural optimizations. The U = 2 and J = 0.7 eV parameters of GGA + U approach were adopted from earlier calculations of LSMO [28–30].

RESULTS AND DISCUSSION

Adsorption of α-6T on the LSMO surface

Topographic AFM images in Figure 1 show the morphological evolution of 6T films grown on the surface of 15 nm thick LSMO films deposited on crystalline STO(100). The bare LSMO surface in Figure 1a shows the typical atomic steps of the STO substrate surface (step height of ~0.4 nm) and exhibits a very flat surface between steps with surface roughness of nearly 0.3 nm, close to the LSMO unit cell [15,31,32]. As shown in Figure 1b – f, 6T films deposited on LSMO follow the Stranski-Krastanov growth mode (2D + 3D) as usually observed for rod-like conjugated molecules deposited on oxides [33]. The first two monolayers (Figure 1b – e) present the Frank – van der Merwe growth mode (2D, layer-by-layer) then for subsequent monolayers up to 6 ML (Figure 1f), the Volmer – Weber growth mode (3D) dominates the film growth.

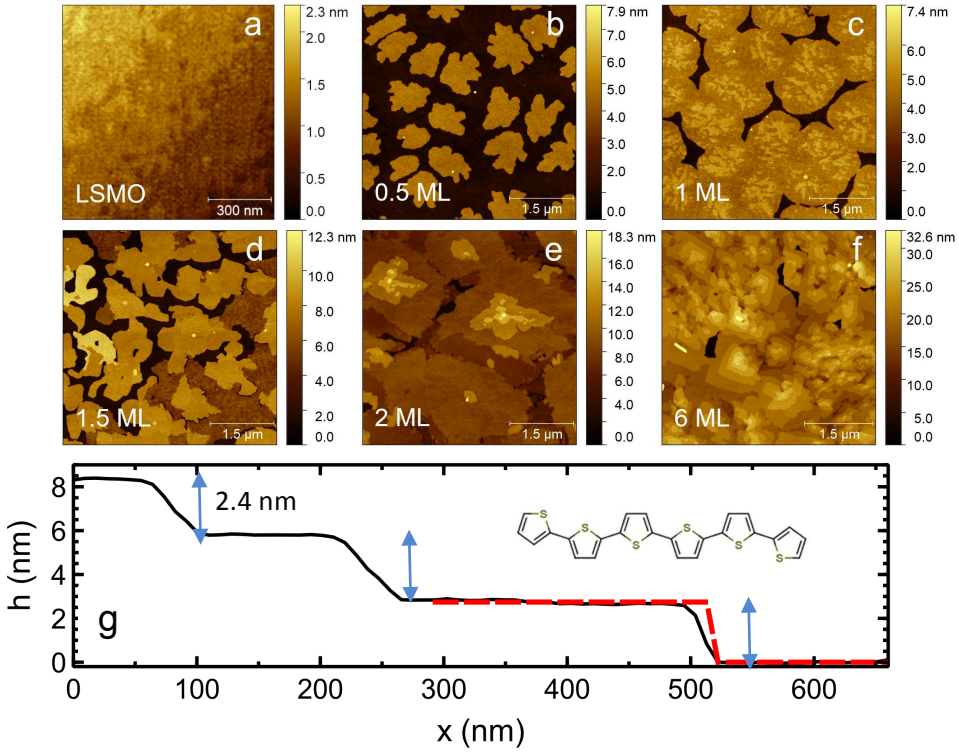

Figure 1: Evolution of 6T morphology for increasing coverage (b-f). Bare LSMO (a). Height profile of the 6 ML thick film (g). The inset in (g) shows the molecular structure of 6T.

In the sub-monolayer regime of 6T deposition, AFM images show the formation of islands (Figure 1b) similarly to what was observed for 6T on silicon oxides [34–36] or other π-conjugated molecules on LSMO [37]. As the thickness increases, the islands expand and eventually coalesce to form an almost complete monolayer (Figure 1c). Notably, on top of 6T islands, the 1 ML-thick film clearly shows aggregates of molecules in the second layer (brighter regions in Figure 1c). By increasing the thickness, i.e. 1.5 ML (Figure 1d), 6T films experience a spontaneous molecular rearrangement (dewetting) [38,39]. Although the dewetting of the film is preserved in the following deposition steps, 2 ML-thick films show the formation of the third and even the fourth ML (Figure 1e), suggesting that the Volmer – Weber growth mode (3D) has started. The profile image (Figure 1g) suggests that the film is formed by upright molecules, with the molecular long axis almost perpendicular to the substrate ~2.4 nm, in analogy to 6T grown on SiO_2 [40] and TiO_2 [41].

Confocal photoluminescence (PL) microscopy

The conformation of molecules on LSMO is confirmed by confocal PL investigations. The PL images corresponding to 1, 2, and 6 ML coverages of 6T on LSMO films are shown in Figure 2a-c. Films are all characterized by low fluorescence quantum yields except red bright spots corresponding to emission from islands of 6T. As expected for the vertical packing of 6T molecules [40,42], the PL spectra of the samples correspond to the emission of an H-type aggregate as shown in Figure 2d. In H-type aggregates, transition moments lie along long molecular axes parallel to one another so that relaxation occurs mainly via nonradiative processes resulting in a low fluorescence quantum yield, in agreement with the low PL intensity detected in our films. Considering the full surface coverage detected by AFM, the presence of dark spots is therefore interpreted as 6T regions with poor dipole coupling resulting in a very weak PL intensity. Such PL quenching is often associated with inhomogeneity in the packing arrangement [ref]. The lack of

new absorption bands or a shift in the spectrum at different coverages indicates that the interface does not originate new excitonic species.

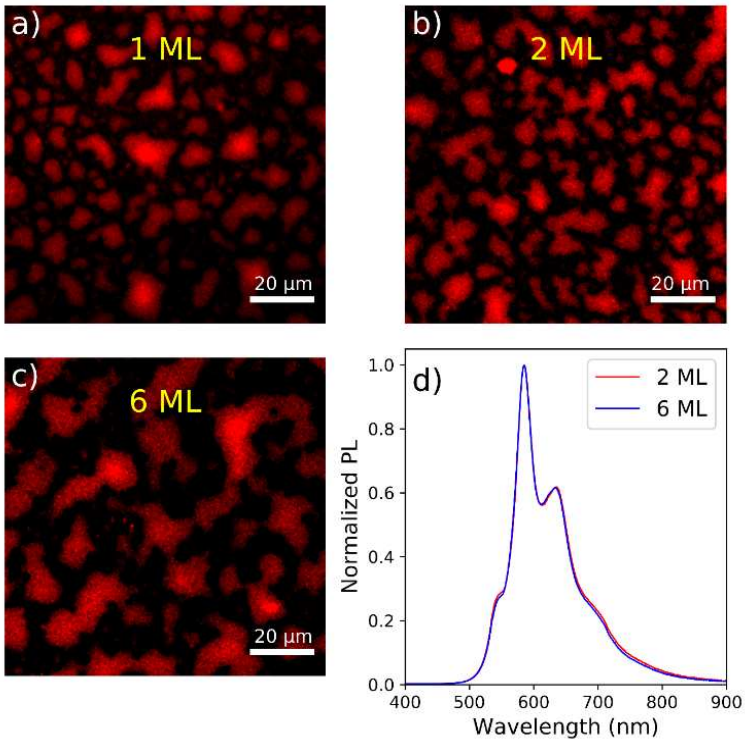

Figure 2. PL images of 1 (a), 2 (b), and 6 (c) ML of T6 on LSMO/STO (λ_{ex} = 488 nm). The PL spectra of 2 ML and 6 ML of T6 on LSMO/STO are also shown (d) (λ_{ex} = 375 nm).

Ultraviolet photoelectron spectroscopy

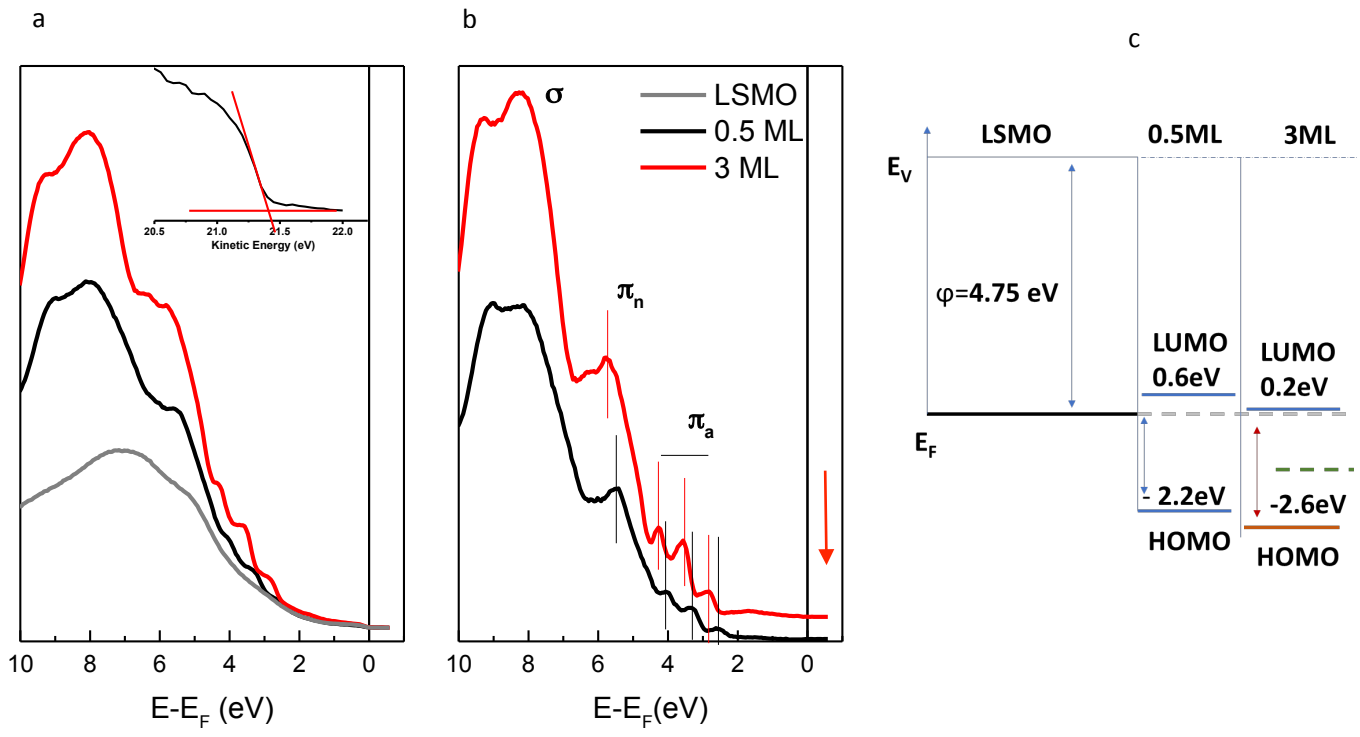

Figure 3. (a) Ultraviolet photoemission spectra of an LSMO surface following incremental growth of sexithiophene films. (b) Spectra obtained by subtraction of the LSMO signal from the total photoemission intensity of the spectra with nominally 0.5 and 3 ML thick 6T overlayers. (c) Band diagram corresponding to the LSMO/6T interface.

We investigate now the energetic configuration at the 6T/LSMO interface. Fig. 3a presents ultraviolet photoemission spectra, collected at normal emission, of the LSMO surface upon incremental growth of sexithiophene films. The spectrum of bare LSMO shows the onset of metallicity at E_F corresponding to Mn e_g states (see inset) and a prominent peak due to emission from O 2*p* and Mn t_{2g} states, in agreement with previous experimental investigations [29] confirming the surface quality of our samples. For the ultrathin 0.5 ML organic layer considered in this study, the UPS spectra consist of contributions from both the organic molecule and the bare LSMO substrate. Therefore, to reveal the contribution of the 6T alone, we subtracted the spectrum of the bare LSMO from the 6T film data, as shown in Figure 3b for 6T coverages of 0.5 ML and 3 ML. The molecular band is already clear at 0.5 ML and both coverages show well-resolved features, as expected for an ordered film and allowing a clear identification of orbital contributions to the density of states (DOS). The peak assignment follows previous studies [43]. The three peaks at around 2–4 eV are the antibonding π_a states; these orbitals are delocalized over the carbon backbone of the molecule, with negligible sulfur contribution [44]; the peak at 5-6 eV is assigned to the nonbonding π states related to localized orbitals of sulphur atoms (π_n), and extended and complex spectral features at 8 eV are ascribed to bonding (σ) states [45]. On increasing coverage from a single molecular layer to multilayer 6T stacks, all peaks shift to a higher energy. We exclude charging effects as the cause of this shift as different features move by different amounts. The onset of the HOMO level, deduced from the onset of emission of the HOMO peak, is measured to be at an energy of 2.2 (2.4) eV relative to the Fermi level for 0.5 ML (3 ML). The position of the lowest unoccupied molecular orbital (LUMO) with respect to the HOMO is deduced from the literature [46] and is close to 2.8 eV. Since the transport gap in the solid state can be larger by several hundreds of meV than the optical gap, our experimental results indicate that E_F is very close but slightly below the LUMO of 6T [47], as depicted in Fig 3c. The position of the LSMO Fermi level with respect to the 6T LUMO favors charge donation from the substrate to the organic molecule.

The shift in position of the work function (φ) with increasing film coverage provides further insight into the strength of the interfacial interaction. The bare LSMO work function was measured to be φ_{LSMO}=4.75eV, as determined from the difference between the excitation energy (*E*=21.2 eV) and the secondary electron emission cut-off. On increasing 6T deposition, a small φ change is observed: for the incomplete coverage (0.5 ML), φ increases by approximately +0.15 eV, and for further 6T deposition (3 ML), the work function decreases and leads to a stabilization of Δφ= +0.05 eV. The adsorbed molecules are reasonably expected to generate a decrease in φ due to the electron push-back effect [48,49]. On the other hand, the presence of charge transfer can cause an increase in the sample work function due to the additional dipole moment induced by the electron transfer from the metal to the molecule. These two competing effects could reasonably explain the scarce change of work function in our bilayer. The small Δφ for the 3 ML sample can be due to multilayer formation, where no further charge transfer occurs, but subtle changes in the monolayer conformation may be induced by multilayer overgrowth. The strength of the interface dipole depends also on the charge-carrier concentration of the substrate. It is important to note that LSMO has a free carrier concentration on the order of 10^{21} cm^{-3} [50], well below the carrier concentration of a standard metal. The appearance of a low intensity broad peak centered at 1.9 eV below E_F for the 3 ML-thick 6T layer (red arrow in Figure 3b) supports this picture of charge transfer [47], in analogy to what has been observed for molecules on doped ZnO [51] where charges from the pseudo-metallic substrate are transferred into the LUMOs. The charge transfer from LSMO to 6T is facilitated by the LUMO position close to E_F however exact quantification is difficult due to the compensating effect of push-back and charge transfer on the work function φ. Note that the electron transfer is likely very small for the 0.5 ML film, inhibiting its observation by UPS.

Metastable de-excitation spectroscopy

MDS is an extremely surface sensitive spectroscopy technique that allows the investigation of the topmost frontier orbitals of the sample. In our case, taking into account the upright orientation of the molecule on LSMO as deduced from AFM and PL spectroscopy, we expect that He 2^3S de-excitation takes place at the terminal thiophene ring. Figure 4a shows the evolution of MDS spectra as 6T is deposited onto the clean LSMO surface. As expected for the helium 2^3S de-excitation process associated with metallic surfaces (resonance ionization followed by Auger neutralization) [52], the bare LSMO layer presents a relatively featureless spectrum. Upon the deposition of the organic molecules, the quasi-one-electron de-excitation process of Auger de-excitation becomes favorable leading to well-defined features associated with HOMO levels. In order to evidence the contribution of the organic phase, the spectrum corresponding to the bare substrate was subtracted due to the incomplete 6T coverage. The peak's assignment follows the description for UPS (see previous section) provided that in MDS the average DOS results from the frontier atoms. The first three peaks (2.8, 3.5 and 4.2 eV) correspond to the antibonding π_a states, which are delocalized over the carbon backbone with negligible coefficients on the sulfur atoms, and are scarcely probed by the He 2^3S beam due to the packing of the 6T island. This explains the low intensity of these components in the spectra. The well-defined peak at 5.8 eV is assigned to nonbonding π_n states from sulfur whose contribution as terminal atoms in the outermost thiophene ring is dominant. The difference in intensity for the components corresponding to the broad peak at 8 eV is associated with an increase of sigma bonds for the 3 ML sample. The direct comparison of UPS and MDS spectra shown in Figure 4b clearly indicates that the position of HOMO states in MDS spectra is similar for both coverages and resembles the 3 ML UPS spectrum. In MDS, the energy spectra of emitted electrons represent the density of states at the very topmost surface of the sample, while UPS, with more penetrating ultraviolet radiation, provides information averaged over the density of states of the entire molecule. This result indicates that the external frontier orbitals of 6T probed by MDS are barely involved in the interaction with LSMO and that only the atomic orbitals at the interface are affected. The calculation of the projected density of states on all the thiophene rings of the molecule under the configuration described in the DFT calculation section (see below) are in agreement with these findings. (see Supplementary S1).

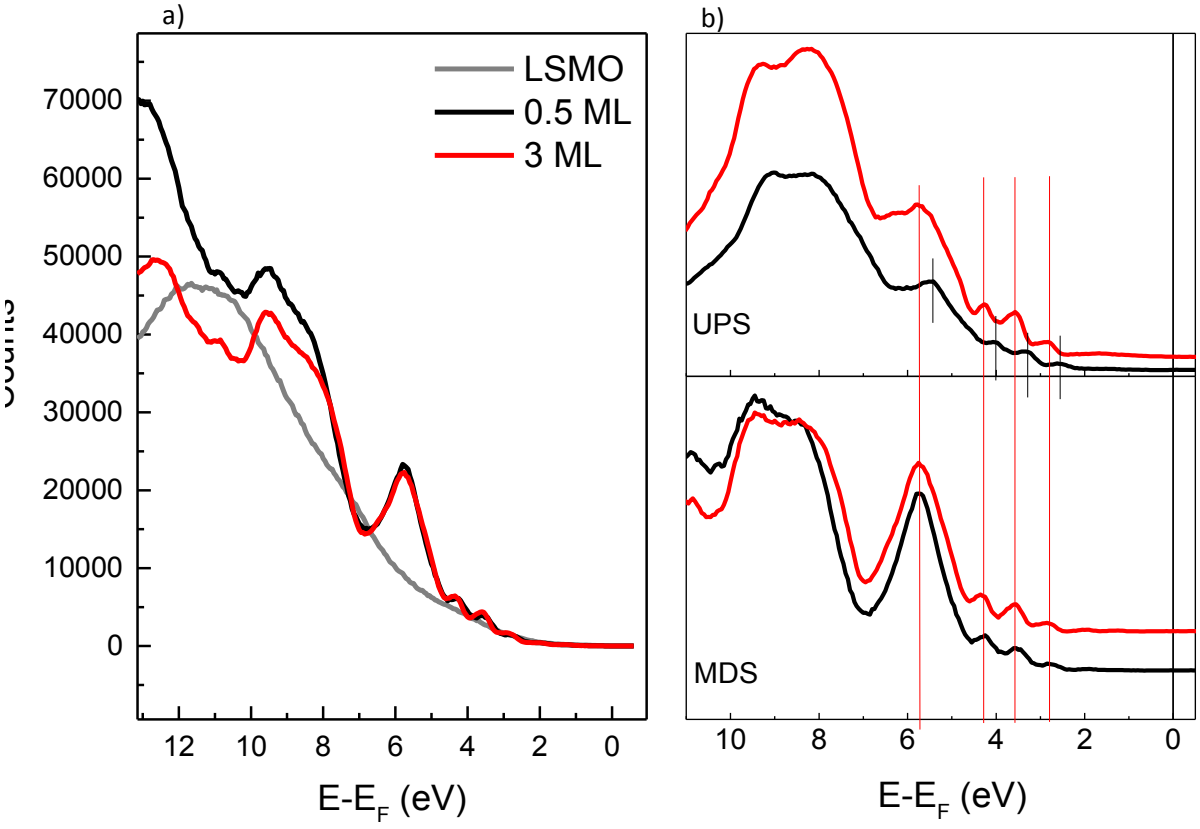

Figure 4. (a) MDS spectra of the LSMO surface upon incremental growth of sexithiophene films. (b) The UPS and MDS spectra are obtained by subtraction of the LSMO signals from the total intensities of the spectra with nominally 0.5 and 3 ML thick 6T overlayers. Lines indicate peak positions for UPS and MDS spectra.

X-ray photoelectron spectroscopy

To understand the interactions between the sulfur headgroups in thiophene and the LSMO surface, we measured the XPS spectra in the S 2p region as a function of coverage. The S 2p XPS spectra are shown in Figure 5. After a Shirley background subtraction, spectra were decomposed into three multiple doublet components with a 1.2 eV spin-orbit splitting reflecting the nonequivalent S atom in the molecule [53]. Considering that 6T adsorbs on LSMO with its long axis upright to the surface, three such S components can be assigned to the central thiol sulfur atoms from the main chain and the two sulfur atoms at the sides, the one close to the surface and the one that is free [54] [55,56]. The lower binding energy peak at 162.7 eV (S1) is typical of sulfide which is presumably S linked to the metal atoms of the LSMO surface [57,58]. This feature is also consistent with partial charge transfer, as observed for aluminum deposition on 6T [58]. Higher binding-energy components (S2 and S3) can be attributed to the thiophene groups not directly interacting with the substrate because their photoemission-induced core holes are not well screened by valence electrons of the substrate [59]. The main S2 component is associated to the thiol sulfur of the chain, while the S3 component to the apical S. Additionally, no sulfur–oxygen bonding is present due to the lack of the corresponding S 2p peak typically appearing at higher binding energy (~168 eV) [60]. Coverage increase from 0.5 ML to 3 ML gives no significant change in binding energy while only a slight change of relative intensities of components is detected. This is consistent with a change in relative weight on increasing the thickness.

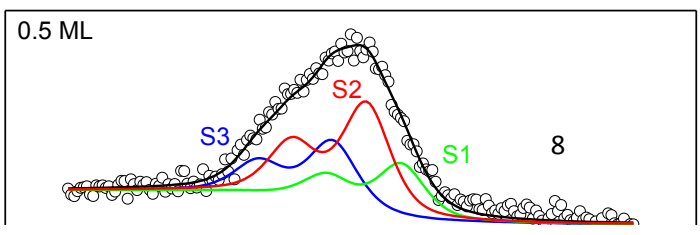

	E (eV)	0.5 ML % Area	3 ML % Area
S1	162.7	0.24	0.19
S2	163.2	0.48	0.55
S3	163.8	0.28	0.26

Figure 5. XPS spectra of the S 2p of sexithiophene films for 0.5 ML (top) and 3 ML (bottom) coverage. Three multiple doublet components (S1 green, S2 red, S3 blue) with a 1.2 eV spin orbit splitting contribute to the full spectrum (data: open circles, fit: black line). Table (right) indicates core level binding energies and population as a function of the coverage.

The effect of the organic deposition on LSMO has been checked by following evolution of Mn 2p photoelectron spectra as a function of 6T coverage. The resulting spectra (see Supplementary S2) are in agreement with data in the literature for LSMO; the line shape remains almost unaffected, indicating that any possible interfacial effects are below the sensitivity in the sampling LSMO volume investigated by XPS.

DFT calculations

In agreement with experimental LSMO surface investigations [12] and following previous theoretical studies [23], both Mn-O and Sr-O terminated LSMO(001) surfaces were considered in possible 6T/LSMO heterostructures. LSMO slabs of six atomic layer thickness with both Mn-O and Sr-O termination layers were produced by cutting the LSMO crystal along the (001) crystallographic plane as depicted in Figure 6. The 4x2 supercell of the LSMO surface was used to calculate the electronic structure of the 6T/LSMO interface with each supercell containing a single 6T molecule coordinated either to the MnO or the SrO surface.

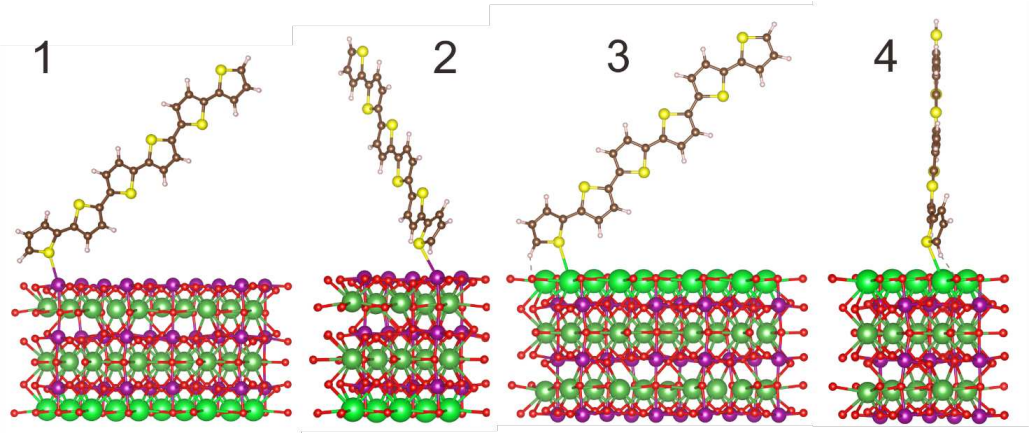

Figure 6. Structure of 6T/LSMO interface with MnO termination (1-2) and SrO termination (3-4). Mn, O, La, Sr, C, and S atoms are depicted in purple, red, green, neon, brown, and yellow, respectively. S atoms are bonded to Mn (1,2) and Sr atoms (3,4).

After structural optimization, the orientation of 6T molecules relative to LSMO/MnO and LSMO/SrO surfaces is determined as ~60^0 inclined with the molecular plane perpendicular to the LSMO(001) surface. Such molecule orientation is consistent with the upright orientation of molecules deduced by AFM and PL spectroscopy. The 6T molecule is coordinated to both MnO and SrO surfaces by a thiol atom with S-Mn and

S-Sr bond lengths equal to 2.85 Å and 3.15 Å which may be characterized as complex and weak dispersion types, respectively. In the case of Sr-O termination, an H-O bond (2.02 Å) can be realized due to a change in the rotational angle with the surface. The distortion of the edge pentagon of 6T is similar for both terminations, as shown in Figure 6, i.e. the contacting pentagon is twisted around a C-C bond while the entire structure remains planar.

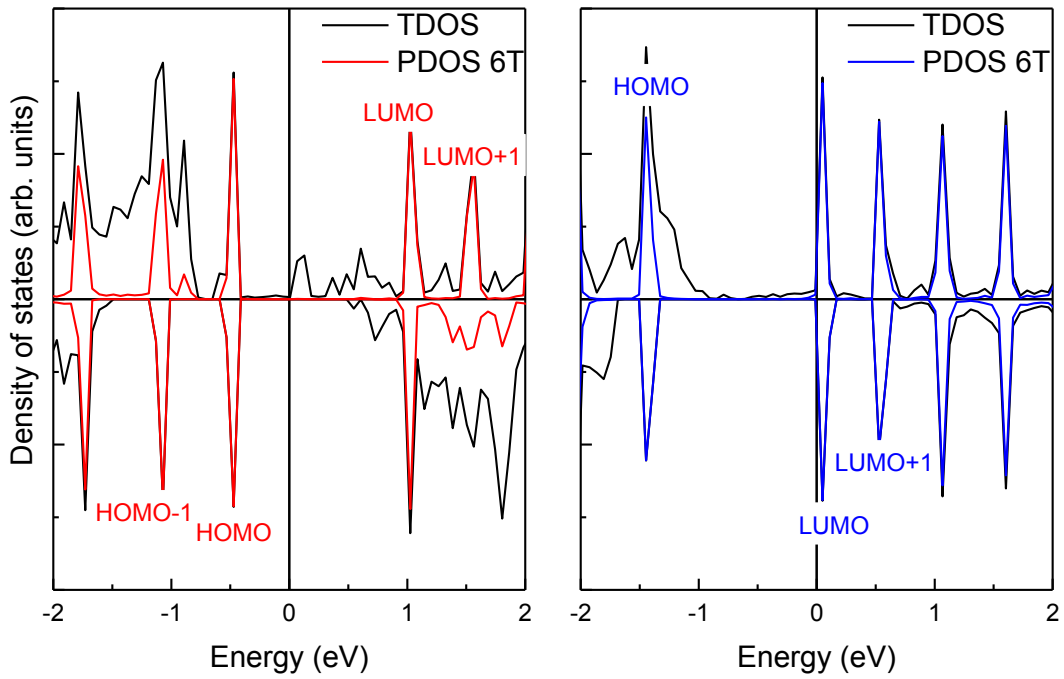

:

Figure 7 (Left) Partial density of states of a 6T molecule (red) and of 6T/LSMO(001)(MnO) with only LSMO atoms in direct contact with 6T (black). (Right) Comparison of the partial density of states of a 6T molecule (blue) and of 6T/LSMO(001)(SrO) with only LSMO atoms in direct contact with 6T (black).

We focus first on MnO-terminated LSMO. In Figure 7 (left), we compare the spin-resolved partial density of states (PDOS) of the 6T molecule adsorbed on the MnO-terminated surface with that corresponding to the LSMO layer considering only the bonding surface atoms. The 6T molecular interaction with the LSMO surface causes a pronounced induced spin polarization of the 6T quasi-molecular LUMO+1 state. The change of 6T in conductivity band due to spin polarization may cause visible asymmetry of intensities of HOMO-LUMO+1 electron transitions for different spin channels. The 6T pseudomolecular spin-up HOMO-1 state coincides in energy with the main LSMO PDOS MnO-layer peak (in the interval -1.1 - -1.3 eV) revealing electronic interactions of LSMO and 6T electronic subsystems. Some interaction of the electronic subsystems is also detected for the secondary LSMO peak at the energy -0.9 eV. Figure 7 (right) displays PDOS of a 6T molecule adsorbed on the SrO-terminated surface with that corresponding to the LSMO layer considering only the bonding surface atoms. Interface interactions of the fragments causes asignificant shift in energy of pseudomolecular 6T HOMO and LUMO states making the LUMO state very close in energy to the Fermi level. The 6T pseudomolecular HOMO state coincides in energy with the most intensive LSMO peak in the spin up channel revealing direct interactions of the spin-up electronic subsystems without causing significant induced spin polarization of 6T.

A comparison of the total DOS for the free-standing 6T molecule with the PDOS for 6T on the MnO-terminated heterostructure is presented in Figure 8 (left). The adsorbed molecule presents a decrease of the HOMO-LUMO gap by 0.08 eV with molecular orbitals shifting down by 0.5 eV. All orbitals (except the HOMO and LUMO) possess high spin-polarisation due to high asymmetry in the distribution of the spin-up and spin-down states. The HOMO-1 state is split into two sub-peaks with a negligible gap between them. For SrO-terminated LSMO, the corresponding configuration does not lead to spin polarization of the 6T (Figure 8 right) with the general shape of the spin-up and spin-down peaks similar to the parent 6T TDOS. A

small decrease of the HOMO-LUMO band gap (15%) is observed but a large shift in the energy of molecular orbitals by 1.4 eV takes place to position the LUMO very close to the Fermi level.

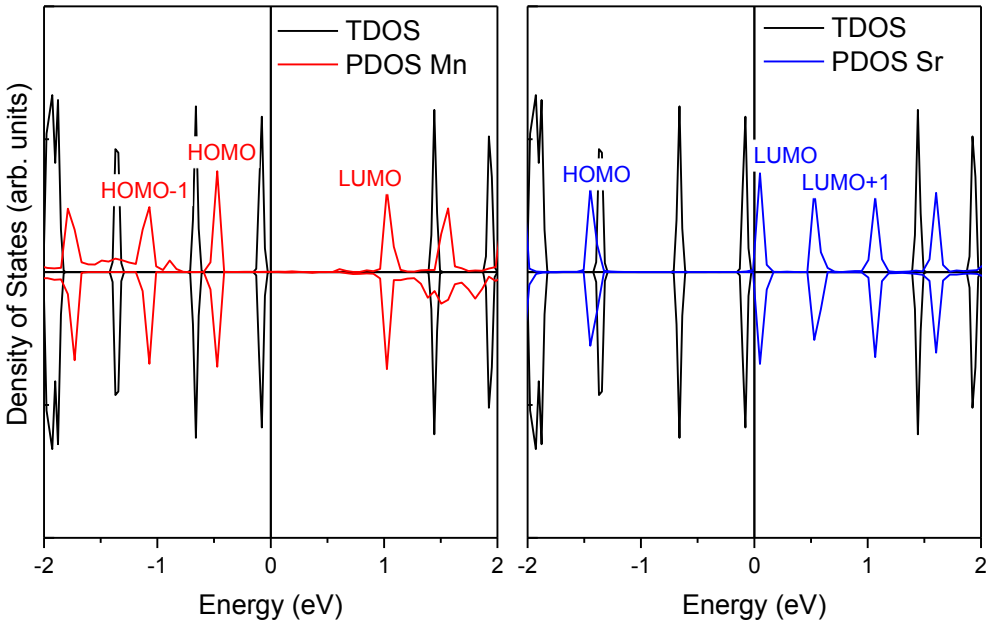

Figure 8. Comparison of TDOS of a free-standing 6T molecule (black) with PDOS of 6T adsorbed on a Mn-O surface (red) (left). (Right) Comparison of TDOS of a free-standing 6T molecule (black) with PDOS of 6T adsorbed on a Sr-O surface (blue).

These results indicate that the LSMO termination layer significantly influences the spin polarization of the 6T molecule. In particular, an effective spin polarization is calculated for 6T adsorption on the MnO termination, while on the SrO termination the electronic properties of the molecule are largely unaffected. The good match of experimental and theoretical results validating the chosen theoretical model is presented in Supplementary Material **S3**.

As demonstrated by detailed surface analysis [12], our LSMO sample features both SrO and MnO terminations. This surface mixture could justify the LUMO position at 0.6 eV from the Fermi level as an intermediate value between the two configurations. Focusing on the LSMO only, the adsorption of the 6T molecule does not affect the spin polarization of the oxide as presented in Figure 9. All orbitals possess a high spin polarisation due to the asymmetry between spin up and spin down states, as expected for the bulk system. LSMO retains its half-metallic nature with an increase in the majority peak intensity at the Fermi level.

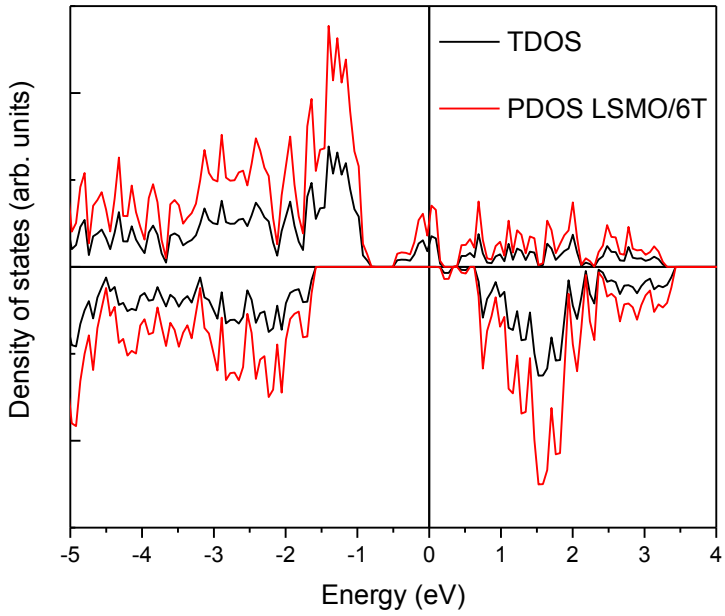

Figure 9. A comparison of the TDOS of pristine LSMO (black) and the LSMO PDOS of a heterostructure with 6T (red).

SUMMARY AND CONCLUSIONS:

Data obtained in this work allow us to describe the typical features of the adsorption of 6T on a ferromagnetic LSMO surface. Importantly, we find that the molecular orbitals of 6T deposited on LSMO are spin polarized and the extent of spin polarization strongly depends on the termination layer of LSMO. Following the trend generally observed for adsorption on oxides, 6T molecules adsorb almost upright on the LSMO surface. The ML formation proceeds via the formation of 6T islands characterized by a quasi vertical stacking of adjacent molecules with π–π orbital interactions of thiophenic rings as detected by confocal PL. Looking in more detail at the interfacial configuration, the most stable geometry calculated by DFT involves the S atoms of the thiophene ring facing the LSMO surface. This is confirmed by the presence of a S 2p component in the XPS spectra associated with the sulfide contribution due to the bond between S and the metal atom of the LSMO. In terms of electronic structure and DOS, the adsorption of 6T onto stoichiometric LSMO surfaces was shown to be characterized by charge transfer from the surface LSMO states into the π-orbitals of the molecule, which is compensated by a push-back effect Pauli repulsion between the metal and molecular electrons. Importantly, no indication of the presence of new electronic states is found in UPS. The surface sensitivity of MDS also reveals that external frontier orbitals are barely involved in the interaction with LSMO and that only the atomic orbitals in close proximity to the interface are affected. Between the possible configurations and binding sites for thiophene adsorption on the two stoichiometric surfaces of LSMO, the Sr-O terminated surface does not impact the spin properties of the interface significantly while the molecular orbitals of 6T linked to the MnO-terminated LSMO surface present spin polarization on the LUMO+1 level. This result enables 6T to act as a spin filtering molecule offering different spin selectivity for majority and minority spins in combination with LSMO.

ACKNOWLEDGEMENT:

This work was financially supported by the Royal Society within the framework of International Exchanges ES\R3\170274 Project “Interfaces with molecular layers: new functionalities for spintronics (INTERFUNS)”. The authors gratefully thank the technical assistance of Mr. Federico Bona.

References

[1] I. Bergenti and V. Dediu, *Spinterface: A New Platform for Spintronics*, Nano Mater. Sci. **1**, 149 (2019).

[2] M. Cinchetti, V. A. Dediu, and L. E. Hueso, *Activating the Molecular Spinterface*, Nat. Mater. **16**, 507 (2017).

[3] F. Djeghloul, M. Gruber, E. Urbain, D. Xenioti, L. Joly, S. Boukari, J. Arabski, H. Bulou, F. Scheurer, F. Bertran, P. Le Fèvre, A. Taleb-Ibrahimi, W. Wulfhekel, G. Garreau, S. Hajjar-Garreau, P. Wetzel, M. Alouani, E. Beaurepaire, M. Bowen, and W. Weber, *High Spin Polarization at Ferromagnetic Metal–Organic Interfaces: A Generic Property*, J. Phys. Chem. Lett. **7**, 2310 (2016).

[4] K. Bairagi, A. Bellec, V. Repain, C. Chacon, Y. Girard, Y. Garreau, J. Lagoute, S. Rousset, R. Breitwieser, Y.-C. Hu, Y. C. Chao, W. W. Pai, D. Li, A. Smogunov, and C. Barreteau, *Tuning the Magnetic Anisotropy at a Molecule-Metal Interface*, Phys. Rev. Lett. **114**, 247203 (6).

[5] A. Droghetti, P. Thielen, I. Rungger, N. Haag, N. Großmann, J. Stöckl, B. Stadtmüller, M. Aeschlimann, S. Sanvito, and M. Cinchetti, *Dynamic Spin Filtering at the Co/Alq 3 Interface Mediated by Weakly Coupled Second Layer Molecules*, Nat. Commun. **7**, 1 (2016).

[6] S. Sanvito, *The Rise of Spinterface Science*, Nat. Phys. **6**, 8 (2010).

[7] Z. H. Xiong, D. Wu, Z. Valy Vardeny, and J. Shi, *Giant Magnetoresistance in Organic Spin-Valves*, Nature **427**, 821 (2004).

[8] V. Dediu, L. E. Hueso, I. Bergenti, A. Riminucci, F. Borgatti, P. Graziosi, C. Newby, F. Casoli, M. P. De Jong, C. Taliani, and Y. Zhan, *Room-Temperature Spintronic Effects in ${\text{Alq}}_{3}$-Based Hybrid Devices*, Phys. Rev. B **78**, 115203 (9).

[9] C. Barraud, P. Seneor, R. Mattana, S. Fusil, K. Bouzehouane, C. Deranlot, P. Graziosi, L. Hueso, I. Bergenti, V. Dediu, F. Petroff, and A. Fert, *Unravelling the Role of the Interface for Spin Injection into Organic Semiconductors*, Nat. Phys. **6**, 615 (2010).

[10] M. P. de Jong, I. Bergenti, V. A. Dediu, M. Fahlman, M. Marsi, and C. Taliani, *Evidence for ${\mathrm{Mn}}^{2+}$ Ions at Surfaces of ${\mathrm{La}}_{0.7}{\mathrm{Sr}}_{0.3}\mathrm{Mn}{\mathrm{O}}_{3}$ Thin Films*, Phys. Rev. B **71**, 014434 (1).

[11] X. Z. Wang, X. M. Ding, Z. S. Li, Y. Q. Zhan, I. Bergenti, V. A. Dediu, C. Taliani, Z. T. Xie, B. F. Ding, X. Y. Hou, W. H. Zhang, and F. Q. Xu, *Modification of the Organic/La0.7Sr0.3MnO3 Interface by in Situ Gas Treatment*, Appl. Surf. Sci. **253**, 9081 (2007).

[12] L. Poggini, S. Ninova, P. Graziosi, M. Mannini, V. Lanzilotto, B. Cortigiani, L. Malavolti, F. Borgatti, U. Bardi, F. Totti, I. Bergenti, V. A. Dediu, and R. Sessoli, *A Combined Ion Scattering, Photoemission, and DFT Investigation on the Termination Layer of a La0.7Sr0.3MnO3 Spin Injecting Electrode*, J. Phys. Chem. C **118**, 13631 (2014).

[13] V. Dediu, M. Murgia, F. C. Matacotta, C. Taliani, and S. Barbanera, *Room Temperature Spin Polarized Injection in Organic Semiconductor*, Solid State Commun. **122**, 181 (2002).

[14] D. Fichou, *Structural Order in Conjugated Oligothiophenes and Its Implications on Opto-Electronic Devices*, J. Mater. Chem. **10**, 571 (2000).

[15] P. Graziosi, M. Prezioso, A. Gambardella, C. Kitts, R. K. Rakshit, A. Riminucci, I. Bergenti, F. Borgatti, C. Pernechele, M. Solzi, D. Pullini, D. Busquets-Mataix, and V. A. Dediu, *Conditions for the Growth of Smooth La0.7Sr0.3MnO3 Thin Films by Pulsed Electron Ablation*, Thin Solid Films **534**, 83 (2013).

[16] A. Pratt, A. Roskoss, H. Ménard, and M. Jacka, *Improved Metastable De-Excitation Spectrometer Using Laser-Cooling Techniques*, Rev. Sci. Instrum. **76**, 053102 (2005).

[17] G. Kresse and J. Furthmüller, *Efficiency of Ab-Initio Total Energy Calculations for Metals and Semiconductors Using a Plane-Wave Basis Set*, Comput. Mater. Sci. **6**, 15 (1996).

[18] G. Kresse and J. Furthmüller, *Efficient Iterative Schemes for Ab Initio Total-Energy Calculations Using a Plane-Wave Basis Set*, Phys. Rev. B **54**, 11169 (10).

[19] G. Kresse and J. Hafner, *Ab Initio Molecular Dynamics for Liquid Metals*, Phys. Rev. B **47**, 558 (Gennaio 1).

[20] G. Kresse and J. Hafner, *Ab Initio Molecular-Dynamics Simulation of the Liquid-Metal--Amorphous-Semiconductor Transition in Germanium*, Phys. Rev. B **49**, 14251 (5).

[21] P. E. Blöchl, *Projector Augmented-Wave Method*, Phys. Rev. B **50**, 17953 (12).

[22] G. Kresse and D. Joubert, *From Ultrasoft Pseudopotentials to the Projector Augmented-Wave Method*, Phys. Rev. B **59**, 1758 (1).

[23] J. P. Perdew, J. A. Chevary, S. H. Vosko, K. A. Jackson, M. R. Pederson, D. J. Singh, and C. Fiolhais, *Atoms, Molecules, Solids, and Surfaces: Applications of the Generalized Gradient Approximation for Exchange and Correlation*, Phys. Rev. B **46**, 6671 (9).

[24] J. P. Perdew, J. A. Chevary, S. H. Vosko, K. A. Jackson, M. R. Pederson, D. J. Singh, and C. Fiolhais, *Erratum: Atoms, Molecules, Solids, and Surfaces: Applications of the Generalized Gradient Approximation for Exchange and Correlation*, Phys. Rev. B **48**, 4978 (8).

[25] V. I. Anisimov, J. Zaanen, and O. K. Andersen, *Band Theory and Mott Insulators: Hubbard U Instead of Stoner I*, Phys. Rev. B **44**, 943 (7).

[26] S. L. Dudarev, G. A. Botton, S. Y. Savrasov, C. J. Humphreys, and A. P. Sutton, *Electron-Energy-Loss Spectra and the Structural Stability of Nickel Oxide: An LSDA+U Study*, Phys. Rev. B **57**, 1505 (1).

[27] S. Grimme, *Semiempirical GGA-Type Density Functional Constructed with a Long-Range Dispersion Correction*, J. Comput. Chem. **27**, 1787 (2006).

[28] C. Ma, Z. Yang, and S. Picozzi, *Ab Initioelectronic and Magnetic Structure in La0.66Sr0.33MnO3: Strain and Correlation Effects*, J. Phys. Condens. Matter **18**, 7717 (2006).

[29] S. Picozzi, C. Ma, Z. Yang, R. Bertacco, M. Cantoni, A. Cattoni, D. Petti, S. Brivio, and F. Ciccacci, *Oxygen Vacancies and Induced Changes in the Electronic and Magnetic Structures of ${\mathrm{La}}_{0.66}{\mathrm{Sr}}_{0.33}\mathrm{Mn}{\mathrm{O}}_{3}$: A Combined Ab Initio and Photoemission Study*, Phys. Rev. B **75**, 094418 (3).

[30] B. Zheng and N. Binggeli, *Influence of the Interface Atomic Structure on the Magnetic and Electronic Properties of ${\text{La}}_{2/3}{\text{Sr}}_{1/3}{\text{MnO}}_{3}/{\text{SrTiO}}_{3}(001)$ Heterojunctions*, Phys. Rev. B **82**, 245311 (12).

[31] P. Graziosi, A. Gambardella, M. Calbucci, K. O'Shea, D. A. MacLaren, A. Riminucci, I. Bergenti, S. Fugattini, M. Prezioso, N. Homonnay, G. Schmidt, D. Pullini, D. Busquets-Mataix, and V. Dediu, *Seed Layer Technique for High Quality Epitaxial Manganite Films*, AIP Adv. **6**, 085109 (2016).

[32] B. Wang, L. You, P. Ren, X. Yin, Y. Peng, B. Xia, L. Wang, X. Yu, S. Mui Poh, P. Yang, G. Yuan, L. Chen, A. Rusydi, and J. Wang, *Oxygen-Driven Anisotropic Transport in Ultra-Thin Manganite Films*, Nat. Commun. **4**, 1 (2013).

[33] G. Hlawacek and C. Teichert, *Nucleation and Growth of Thin Films of Rod-like Conjugated Molecules*, J. Phys. Condens. Matter **25**, 143202 (2013).

[34] C. Albonetti, M. Barbalinardo, S. Milita, M. Cavallini, F. Liscio, J.-F. Moulin, and F. Biscarini, *Selective Growth of α-Sexithiophene by Using Silicon Oxides Patterns*, Int. J. Mol. Sci. **12**, 9 (2011).

[35] J.-F. Moulin, F. Dinelli, M. Massi, C. Albonetti, R. Kshirsagar, and F. Biscarini, *In Situ X-Ray Synchrotron Study of Organic Semiconductor Ultra-Thin Films Growth*, Nucl. Instrum. Methods Phys. Res. Sect. B Beam Interact. Mater. At. **246**, 122 (2006).

[36] F. Dinelli, M. Murgia, P. Levy, M. Cavallini, F. Biscarini, and D. M. de Leeuw, *Spatially Correlated Charge Transport in Organic Thin Film Transistors*, Phys. Rev. Lett. **92**, 116802 (2004).

[37] P. Graziosi, A. Riminucci, M. Prezioso, C. Newby, D. Brunel, I. Bergenti, D. Pullini, D. Busquets-Mataix, M. Ghidini, and V. A. Dediu, *Pentacene Thin Films on Ferromagnetic Oxide: Growth Mechanism and Spintronic Devices*, Appl. Phys. Lett. **105**, 022401 (2014).

[38] S. A. Burke, J. M. Topple, and P. Grutter, *Molecular Dewetting on Insulators*, J Phys 17 (2009).

[39] D. Käfer, C. Wöll, and G. Witte, *Thermally Activated Dewetting of Organic Thin Films: The Case of Pentacene on SiO2 and Gold*, Appl. Phys. A **95**, 273 (2009).

[40] F. Dinelli, J.-F. Moulin, M. A. Loi, E. Da Como, M. Massi, M. Murgia, M. Muccini, F. Biscarini, J. Wie, and P. Kingshott, *Effects of Surface Chemical Composition on the Early Growth Stages of α-Sexithienyl Films on Silicon Oxide Substrates*, J. Phys. Chem. B **110**, 258 (2006).

[41] J. Ivanco, T. Haber, J. R. Krenn, F. P. Netzer, R. Resel, and M. G. Ramsey, *Sexithiophene Films on Ordered and Disordered TiO2(110) Surfaces: Electronic, Structural and Morphological Properties*, Surf. Sci. **601**, 178 (2007).

[42] M. A. Loi, E. da Como, F. Dinelli, M. Murgia, R. Zamboni, F. Biscarini, and M. Muccini, *Supramolecular Organization in Ultra-Thin Films of α-Sexithiophene on Silicon Dioxide*, Nat. Mater. **4**, 81 (2005).

[43] S. Ohno, H. Tanaka, K. Tanaka, K. Takahashi, and M. Tanaka, *Electronic Structure of α-Sexithiophene Ultrathin Films Grown On*, Phys. Chem. Chem. Phys. **20**, 1114 (2018).

[44] M. Lögdlund, P. Dannetun, C. Fredriksson, W. R. Salaneck, and J. L. Brédas, *Theoretical and Experimental Studies of the Interaction between Sodium and Oligothiophenes*, Phys. Rev. B **53**, 16327 (1996).

[45] H. Fujimoto, U. Nagashima, H. Inokuchi, K. Seki, Y. Cao, H. Nakahara, J. Nakayama, M. Hoshino, and K. Fukuda, *Ultraviolet Photoemission Study of Oligothiophenes: Π-band Evolution and Geometries*, J. Chem. Phys. **92**, 4077 (1990).

[46] C. Taliani and L. M. Blinov, *The Electronic Structure of Solid α-Sexithiophene*, Adv. Mater. **8**, 353 (1996).

[47] S. Duhm, H. Glowatzki, V. Cimpeanu, J. Klankermayer, J. P. Rabe, R. L. Johnson, and N. Koch, *Weak Charge Transfer between an Acceptor Molecule and Metal Surfaces Enabling Organic/Metal Energy Level Tuning*, J. Phys. Chem. B **110**, 21069 (2006).

[48] R. Otero, A. L. Vázquez de Parga, and J. M. Gallego, *Electronic, Structural and Chemical Effects of Charge-Transfer at Organic/Inorganic Interfaces*, Surf. Sci. Rep. **72**, 105 (2017).

[49] S. Braun, W. R. Salaneck, and M. Fahlman, *Energy-Level Alignment at Organic/Metal and Organic/Organic Interfaces*, Adv. Mater. **21**, 1450 (2009).

[50] I. Bergenti, V. Dediu, E. Arisi, T. Mertelj, M. Murgia, A. Riminucci, G. Ruani, M. Solzi, and C. Taliani, *Spin Polarised Electrodes for Organic Light Emitting Diodes*, Org. Electron. **5**, 309 (2004).

[51] S. Erker and O. T. Hofmann, *Fractional and Integer Charge Transfer at Semiconductor/Organic Interfaces: The Role of Hybridization and Metallicity*, J. Phys. Chem. Lett. **10**, 848 (2019).

[52] A. Pratt, L. Dunne, X. Sun, M. Kurahashi, and Y. Yamauchi, *Energy-Level Alignment at the Alq3/Fe3O4(001) Interface*, J. Appl. Phys. **111**, 07C114 (2012).

[53] G. Horowitz, B. Bachet, A. Yassar, P. Lang, F. Demanze, J.-L. Fave, and F. Garnier, *Growth and Characterization of Sexithiophene Single Crystals*, Chem. Mater. **7**, 1337 (1995).

[54] T. Jiang, W. Malone, Y. Tong, D. Dragoe, A. Bendounan, A. Kara, and V. A. Esaulov, *Thiophene Derivatives on Gold and Molecular Dissociation Processes*, J. Phys. Chem. C **121**, 27923 (2017).

[55] J. Jia, A. Kara, L. Pasquali, A. Bendounan, F. Sirotti, and V. A. Esaulov, *On Sulfur Core Level Binding Energies in Thiol Self-Assembly and Alternative Adsorption Sites: An Experimental and Theoretical Study*, J. Chem. Phys. **143**, 104702 (2015).

[56] O. Baseggio, D. Toffoli, M. Stener, G. Fronzoni, M. de Simone, C. Grazioli, M. Coreno, A. Guarnaccio, A. Santagata, and M. D'Auria, *S2p Core Level Spectroscopy of Short Chain Oligothiophenes*, J. Chem. Phys. **147**, 244301 (2017).

[57] L. Sang and J. E. Pemberton, *Chemistry at the Interface of α-Sexithiophene and Vapor-Deposited Ag, Al, Mg, and Ca: A Molecular View*, J. Phys. Chem. C **123**, 18877 (2019).

[58] R. Lazzaroni, J. L. Brédas, P. Dannetun, M. Lögdlund, K. Uvdal, and W. R. Salaneck, *Electronic Structure of the Aluminum/Polythiophene Interface: A Joint Experimental and Theoretical Study*, Synth. Met. **43**, 3323 (1991).

[59] A. Nambu, H. Kondoh, I. Nakai, K. Amemiya, and T. Ohta, *Film Growth and X-Ray Induced Chemical Reactions of Thiophene Adsorbed on Au(111)*, Surf. Sci. **530**, 101 (2003).

[60] R. A. Walton, *The X-Ray Photoelectron Spectra of Metal Complexes of Sulfur-Containing Ligands: Sulfur 2p Binding Energies*, Coord. Chem. Rev. **31**, 183 (1980).